LISA Galactic binaries with astrometry from Gaia DR3

Thomas Kupfer [ID],[1] Valeriya Korol [ID],[2,3]

both authors contributed equally to this work

Tyson B. Littenberg,[4] Sweta Shah [ID],[5,6] Etienne Savalle [ID],[7] Paul J. Groot,[8,9,10] Thomas R. Marsh [ID],[11]
Maude Le Jeune,[7] Gijs Nelemans,[12,13,14] Antoine Petiteau [ID],[7,15] Gavin Ramsay [ID],[16] Danny Steeghs [ID],[11]
Stanislav Babak,[7]

[1]Department of Physics and Astronomy, Texas Tech University, PO Box 41051, Lubbock, TX 79409, USA
[2]Max-Planck-Institut für Astrophysik, Karl-Schwarzschild-Straße 1, 85741 Garching, Germany
[3]Institute for Gravitational Wave Astronomy, School of Physics and Astronomy, University of Birmingham, Birmingham, B15 2TT, UK
[4]NASA Marshall Space Flight Center, Huntsville, Alabama 35811, USA
[5]Max Planck Institute for Gravitational Physics (Albert Einstein Institute), Callinstrasse 38, 30167 Hannover, Germany
[6]Leibniz Universität Hannover, Institut für Gravitationsphysik, Callinstrasse 38, 30167 Hannover, Germany
[7]Universitdé Paris, CNRS, Astroparticule et Cosmologie, 75013 Paris, France
[8]Department of Astrophysics/IMAPP, Radboud University, P.O.Box 9010, 6500 GL Nijmegen, The Netherlands
[9]South African Astronomical Observatory, PO Box 9, Observatory, 7935, Cape Town, South Africa
[10]Department of Astronomy & Inter-University Institute for Data Intensive Astronomy, University of Cape Town, Private Bag X3, 7701 Rondebosch, South Africa
[11]Department of Physics, University of Warwick, Gibbet Hill Road, Coventry CV4 7AL, UK
[12]Department of Astrophysics/IMAPP, Radboud University, P.O. Box 9010, 6500 GL Nijmegen, The Netherlands
[13]SRON, Netherlands Institute for Space Research, Niels Bohrweg 4, 2333 CA Leiden, The Netherlands
[14]Institute of Astronomy, KU Leuven, Celestijnenlaan 200D, B-3001 Leuven, Belgium
[15]IRFU, CEA, Université Paris-Saclay, F-91191, Gif-sur-Yvette, France
[16]Armagh Observatory and Planetarium, College Hill, Armagh BT61 9DG, UK

ABSTRACT

Galactic compact binaries with orbital periods shorter than a few hours emit detectable gravitational waves at low frequencies. Their gravitational wave signals can be detected with the future *Laser Interferometer Space Antenna* (*LISA*). Crucially, they may be useful in the early months of the mission operation in helping to validate *LISA*'s performance in comparison to pre-launch expectations. We present an updated list of 48 candidate *LISA* binaries with measured properties, for which we derive distances based on *Gaia* Data release 3 astrometry. Based on the known properties from electromagnetic observations, we predict the *LISA* detectability after 1, 3, 6, and 48 months with state-of-the-art Bayesian analysis methods. We distinguish between verification and detectable binaries as being detectable after 3 and 48 months respectively. We find 16 verification binaries and 21 detectable sources, which triples the number of known *LISA* binaries over the last few years. These include detached double white dwarfs, AM CVn binaries, one ultracompact X-ray binary and two hot subdwarf binaries. We find that across this sample the gravitational wave amplitude is expected to be measured to $\approx 10\%$ on average, while the inclination is expected to be determined with $\approx 15°$ precision. For detectable binaries these average errors increase to $\approx 50\%$ and to $\approx 40°$ respectively.

Keywords: TBD

1. INTRODUCTION

Binary systems composed of degenerate stellar remnants (white dwarfs, neutron stars and black holes) in orbits with periods of less than a few hours are predicted to be strong gravitational wave (GW) sources in our own Galaxy. Perhaps the most prominent example of such a system is the first binary pulsar discovered by Hulse & Taylor (1975), which via the measurement of its orbital decay over three decades, led to the first indirect evidence for the existence

of GWs (Weisberg & Taylor 2005) and paved the way forward for the field of GW astronomy. Since then, many more systems consisting of a neutron star/white dwarf with a compact helium-star/white dwarf/neutron star companion with orbital periods as short as several minutes have been discovered, mainly at optical or X-ray electromagnetic (EM) wavebands (e.g. Amaro-Seoane et al. 2022). Binaries in a such a tight orbit emit GWs at mHz frequencies that can be detected directly with the future *Laser Interferometer Space Antenna* (*LISA*, Amaro-Seoane et al. 2017), and other future planned space-based GW observatories such as *TianQin* (Luo et al. 2016; Huang et al. 2020), *Taiji* (Ruan et al. 2018) and the *Lunar Gravitational Wave Antenna* (Harms et al. 2021).

In this study we focus on the *LISA* mission, which is a European Space Agency (ESA)-led GW observatory currently scheduled for launch in the mid-2030s[1]. Designed to operate in the frequency band between 0.1 mHz and 100 mHz (Amaro-Seoane et al. 2017), *LISA* is an ideal tool for discovering massive black hole mergers and extreme-/intermediate-mass ratio inspirals. In addition, it can survey the shortest period stellar remnant binaries throughout the entire Milky Way, providing a complementary view of our Galaxy to EM surveys (for a review see Amaro-Seoane et al. 2022). Both theory- and observation-based studies find that *LISA* will deliver a sample of $\mathcal{O}(10^4)$ binaries with orbital periods of < 1 hour, which will be complete up to periods of < 15 min (e.g. Nelemans et al. 2001; Ruiter et al. 2009; Nissanke et al. 2012; Lamberts et al. 2019; Breivik et al. 2020; Li et al. 2020; Korol et al. 2022). A significant number of $\mathcal{O}(10^2)$ of stellar remnant binaries – primarily those composed of two white dwarfs – discovered by *LISA* will be possible to study in combination with EM surveys (e.g. Nelemans et al. 2004; Marsh 2011; Korol et al. 2017; Breivik et al. 2018; Tauris 2018; Li et al. 2020).

In the context of the *LISA* mission, stellar remnant binaries known from EM observations are often termed 'verification binaries', based on the idea that one can model their GW signal using EM measurements of binary's parameters and to employ these to test *LISA* data quality (e.g. Ströer & Vecchio 2006; Littenberg 2018; Savalle et al. 2022). In our previous work, we reviewed a sample of candidate *LISA* verification binaries following the second *Gaia* data release (DR2). This allowed us to determine distances – previously highly uncertain for most binaries – based on *Gaia*'s parallax measurements (Kupfer et al. 2018; Ramsay et al. 2018). In turn, new distance estimates enabled us to evaluate the uncertainty on the expected GW signal's amplitude and to assess the detectability of these candidate verification binaries with *LISA*. In this work we update the sample of candidates *LISA* verification binaries in a number of ways. Firstly, we include several newly discovered systems since *Gaia* DR2 (Section 2). Secondly, we re-evaluate the distances based on improved astrometry from the third *Gaia* DR3, while also taking into account their proper motion information (Section 3.2). In addition, we evaluate their detectability as well as the binary parameter estimation in a fully-Bayesian way using the up-to-date *LISA* sensitivity requirements (Section 3.3).

So far verification binaries have been (arbitrarily) defined as such based on an assumed signal-to-noise ratio (SNR) detection threshold reached at a set observation time. However, this definition relies on a few caveats. Firstly, the SNR threshold and the integration time needed to make an unambiguous identification of a (known) source is not just a matter of its intrinsic amplitude, but is heavily dependent on the realization of the rest of the Galactic population (i.e. unresolved Galactic confusion foreground) that the source is competing against. The Galactic confusion foreground is a dynamical quantity: it will decrease with time as more and more sources will become detectable and will be "subtracted" from the foreground. In addition, *LISA*'s orbit around the Sun will introduce a modulation in the Galactic foreground reaching its maximum when *LISA* is optimally oriented towards the Galactic center, which is where the density of Galactic sources peaks (e.g. Petiteau 2008). A prototype global fit data analysis pipeline for *LISA* demonstrated that the Galactic foreground subtraction steadily improves with time with a few $\mathcal{O}(10^3)$ binaries being identified (and subtracted) already after 1 month (Littenberg & Cornish 2023). Moreover, known binaries will be the most crucial in the early weeks/months of the mission operation in helping to validate the early performance of the instrument in comparison to pre-launch expectations. It is therefore reasonable to expect that the first data validation may be required after only a few months from the beginning of science operations, e.g. to guarantee the first data release within six months - one year of mission. We note that the data release scenario for *LISA* is still to be defined by ESA. We anticipate that an integration time as short as 1-3 months would allow for basic consistency tests on the recovered parameters on a few epochs of commissioning data for several verification binaries. Given all the above, in this study we opt to call as *verification binary* a system that becomes detectable, which is judged based on the shape of the recovered posteriors on binary's parameters rather than a SNR threshold, within 3 months of observation time
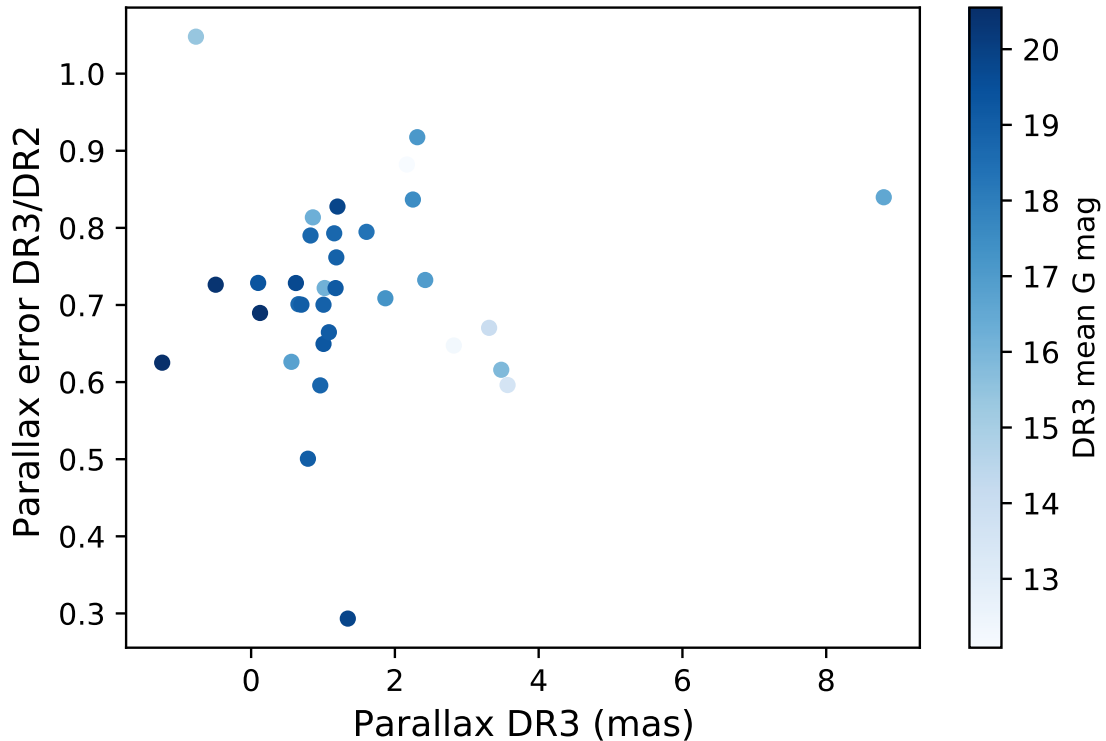
---

[1] https://sci.esa.int/web/lisa/-/61367-mission-summary

Figure 1. The error of the parallax in DR3 compared to DR2 for the LISA verification sources in Tables 1 and 2. The colour indicates the mean G mag of the source.

with *LISA*, and we call a as *detectable binary* when it is detected after 48 months (at present set as the nominal lifetime of the mission).

2. THE SAMPLE OF COMPACT *LISA* SOURCES SINCE GAIA DR2

At present the catalog of candidate verification binaries includes detached (Brown et al. 2016a) and semi-detached double white dwarfs (the latter called AM CVn type binaries; see Solheim (2010) for a recent review), hot subdwarf stars with a white dwarf companion (see Geier et al. (2013); Kupfer et al. (2022); Pelisoli et al. (2021) for recent discoveries), semi-detached white dwarf-neutron star binaries (so-called ultracompact X-ray binaries; Nelemans & Jonker 2010) and double neutron stars (Lyne et al. 2004).

In Kupfer et al. (2018) we analyzed ~ 50 known candidates using distances derived from parallaxes provided in the *Gaia* DR2 catalog (DR2, Gaia Collaboration et al. 2018). We found that 13 candidates exceed a signal-to-noise threshold of 5 for a LISA mission duration of 4 years.

Over the past few years large scale sky surveys have increased the number of compact binaries substantially. The Zwicky Transient Facility (ZTF) performed a dedicated high-cadence survey to find short period binaries (Kupfer et al. 2021). As many as 20 new binary systems with orbital periods ranging from 7 min to $\approx 1\,$h have been discovered by ZTF since the beginning of science operations in March 2018 (Bellm 2014; Burdge et al. 2019a, 2020a,b; Kupfer et al. 2020a,b; van Roestel et al. 2022). This new sample includes seven eclipsing systems, seven AM CVn systems, and six systems exhibiting primarily ellipsoidal variations in their light curves. Remarkably, one of the first ZTF discoveries was the shortest orbital period eclipsing binary system known to date, ZTF J1539+5027, with an orbital period of just 6.91 min (Burdge et al. 2019a). Owing both to its inherently high GW frequency and large GW amplitude, ZTF J1539+5027 is expected to be one of the loudest Galactic GW sources and could reach the signal-to-noise detection threshold of ≈ 7 within a week. Littenberg & Cornish (2019) showed that for high frequency systems like ZTF J1539+5027, GW measurements will independently provide comparable levels of precision to the current EM measurement of the orbital evolution of the system, and will improve the precision to which the distance and orientation is known.
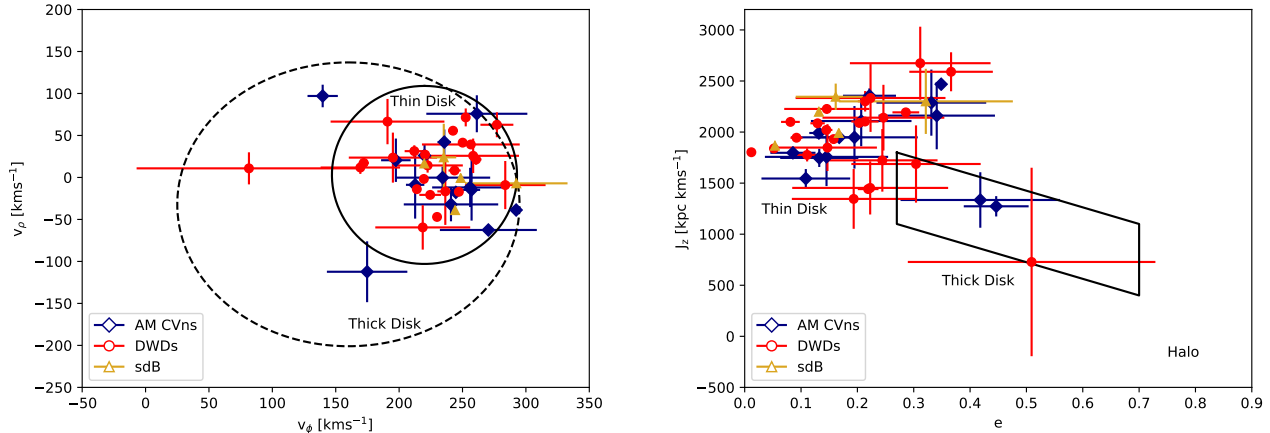
Figure 2. $V_\phi - V_\rho$ (left) and $e - J_z$ diagrams (right). The solid and dotted ellipses render the 3σ thin and thick disk contours in the $V_\phi - V_\rho$ diagram, while the solid box in the $e - J_z$ marks the thick disk region as specified by Pauli et al. (2006)

The Extremely low mass (ELM) white dwarf survey finished their observatons over the SDSS footprint (Brown et al. 2022) and expanded their search to the Southern hemisphere (Kosakowski et al. 2020). Over the last few years the ELM survey discovered several sub-hour orbital-period double degenerates, including the first double helium-core white dwarf binary (e.g. Brown et al. 2020; Kilic et al. 2021; Kosakowski et al. 2021). It is expected that double helium-core white dwarfs and carbon/oxygen + helium-core white dwarfs dominate the population in the *LISA* band despite that they make up only 10 per cent of the global double white dwarf population (Lamberts et al. 2019).

Moreover, several additional candidates have been found in other large-scale surveys. SDSS J1337 was discovered as a double degenerate in early SDSS-V data with an orbital period of 99 min. The spectrum shows spectral lines from both components making it a double lined system which provides precise system parameters (Chandra et al. 2021). Pelisoli et al. (2021) discovered a compact hot subdwarf binary with a massive white dwarf companion in a 99 min period orbit in the TESS sky survey. The total mass of the system is above the Chandrasekhar mass making the system a double degenerate supernova Ia progenitor.

The large number of sky surveys tripled the number of candidate compact binaries over the last few years since the release of Gaia DR2. However, different types of surveys use different detection techniques and analysis methods. This leads to a non-uniformity in the way results are presented. Table 1 presents an overview of observational results of the known *LISA* detectable sources as they are reported by the respective studies. Properties for all sources collected for this publication are publicly available on the *LISA* Consortium GitLab repository https://gitlab.in2p3.fr/LISA/lisa-verification-binaries.

3. METHODS

3.1. *Improvements from Gaia DR2 to Gaia DR3*

In 2018 Gaia DR2 released full astrometric solutions, including parallaxes, and proper motions of 1.3 billion sources (Gaia Collaboration et al. 2016, 2018). The release was based on observations taken between July 2014 and May 2016. The parallaxes allowed us for the first time to calculate distances for a large sample of *LISA* detectable compact binaries. The distances in combination with the chirp mass provided the opportunity to calculate gravitational wave amplitudes and estimate the detectability for *LISA* (Kupfer et al. 2018). Until Gaia DR2 only a small sample of AM CVn binaries had parallax measurements using the Hubble Space telescope (Roelofs et al. 2007a).

About two years after the second data release, the Gaia early data release (eDR3) provided full astrometric solutions of 1.4 billion sources based on 34 month of observations (Gaia Collaboration et al. 2020). The released data included one additional year of Gaia data leading to a higher precision in the parallaxes and proper motions compared to DR2 as well as first time parallax measurements for several *LISA* sources, including ZTFJ1905, SDSSJ0935, V803 Cen and CR Boo. Generally, we find that the parallaxes improved by about 20% - 30% between DR2 and eDR3, in particular for faint sources (Fig. 1).

Table 1. Physical properties of the known verification and detectable binaries. Masses and inclination angles in brackets are assumed and based on evolutionary stage and mass ratio estimations. Absolute magnitudes are calculated from the Gaia G-band magnitude in combination with our distance estimate.

Source	Type	Orbital period (s)	$l_{\rm Gal}$ (deg)	$b_{\rm Gal}$ (deg)	BP-RP (mag)	$M_{\rm G}$ (mag)	m_1 (M$_\odot$)	m_2 (M$_\odot$)	ι (deg)
Verification binaries									
HM Cnc[1,2]	AMCVn	321.529129(10)	206.9246	23.3952	0.246	6.54	0.55	0.27	$\approx$38
ZTFJ1539[3]	DWD*	414.7915404(29)	80.7746	50.5819	-0.263	8.44	$0.61^{+0.017}_{-0.022}$	0.21 ± 0.015	$84.15^{+0.64}_{-0.57}$
ZTFJ2243[4]	DWD*	527.934890(32)	104.1514	-5.4496	-0.160	9.33	$0.349^{+0.093}_{-0.074}$	$0.384^{+0.114}_{-0.074}$	$81.88^{+1.31}_{-0.69}$
V407 Vul[5]	AMCVn	569.396230(126)	57.7281	6.4006	1.535	7.76	[0.8$\pm$0.1]	[0.177$\pm$0.071]	[60]
ES Cet[6]	AMCVn*	620.21125(30)	168.9684	-65.8632	-0.296	5.55	[0.8$\pm$0.1]	[0.161$\pm$0.064]	[60]
SDSSJ0651*[7,8]	DWD*	765.206543(55)	186.9277	12.6886	0.029	9.37	0.247$\pm$0.015	0.49$\pm$0.02	$86.9^{+1.6}_{-1.0}$
ZTFJ0538[9]	DWD*	866.60331(16)	186.8104	-6.2213	0.025	8.80	0.45 ± 0.05	0.32 ± 0.03	$85.43^{+0.07}_{-0.09}$
SDSSJ1351[10]	AMCVn	939.0(7.2)	328.5021	53.1240	-0.122	7.80	[0.8$\pm$0.1]	[0.100$\pm$0.040]	[60]
AM CVn[11,12]	AMCVn	1028.7322(3)	140.2343	78.9382	-0.283	6.66	0.68$\pm$0.06	0.125$\pm$0.012	43$\pm$2
ZTFJ1905[9]	AMCVn*	1032.16441(62)	0.1945	1.0968	-0.066	11.47	[0.8$\pm$0.1]	[0.090$\pm$0.035]	70 ± 20
SDSSJ1908[13,14]	AMCVn	1085.108(1)	70.6664	13.9349	-0.018	6.27	[0.8$\pm$0.1]	[0.085$\pm$0.034]	10 - 20
HP Lib[15,16]	AMCVn	1102.70(5)	352.0561	32.5467	-0.153	6.36	0.49-0.80	0.048-0.088	26-34
SDSSJ0935[17,18]	DWD	1188(42)	176.0796	47.3776	0.455	9.82	0.312$\pm$0.019	0.75$\pm$0.24	[60]
J1239-2041[19]	DWD	1350.432(11.232)	299.2755	42.0943	-0.072	9.00	0.291 ± 0.013	$0.68^{+0.11}_{-0.06}$	71^{+8}_{-10}
SDSS0634[20]	DWD	1591.4(28.9)	176.7322	13.3211	-0.189	8.95	$0.452^{+0.070}_{-0.062}$	$0.209^{+0.034}_{-0.021}$	37 ± 7
V803 Cen[16,21]	AMCVn	1596.4(1.2)	309.3671	20.7262	0.232	8.44	0.78-1.17	0.059-0.109	12 - 15
Detectable binaries									
4U1820–30[22,23]	UCXB	685(4)	2.7896	-7.9144	-	3.7[42]	[1.4]	[0.069]	[60]
SDSSJ2322[24]	DWD	1201.4(5.9)	85.9507	-51.2104	-0.179	9.08	0.34 ± 0.02	> 0.17	[60]
PTFJ0533[25]	DWD	1233.97298(17)	201.8012	-16.2238	-0.067	8.70	$0.652^{+0.037}_{-0.040}$	0.167 ± 0.030	$72.8^{+0.8}_{-1.4}$
ZTFJ2029[9]	DWD*	1252.056499(41)	58.5836	-13.4655	-0.054	10.27	0.32 ± 0.04	0.30 ± 0.04	$86.64^{+0.70}_{-0.40}$
PTF1J1919[26]	AMCVn*	1347.354(20)	79.5945	15.5977	0.036	9.08	[0.8$\pm$0.1]	[0.066$\pm$0.026]	[60]
CXOGBSJ1751[27]	AMCVn	1374.0(6)	359.9849	-1.4108	1.623	6.01	[0.8$\pm$0.1]	[0.064$\pm$0.026]	[60]
ZTFJ0722[9]	DWD*	1422.548655(71)	232.9930	-1.8604	-0.157	8.23	0.38 ± 0.04	0.33 ± 0.03	89.66 ± 0.22
CR Boo[16,28]	AMCVn	1471.3056(500)	340.9671	66.4884	0.066	7.74	0.67-1.10	0.044-0.088	30
KL Dra[29]	AMCVn	1501.806(30)	91.0140	19.1992	0.668	9.25	0.76	0.057	[60]
PTF1J0719[30]	AMCVn	1606.2(1.2)	168.6573	24.4945	0.425	9.30	[0.8$\pm$0.1]	[0.053$\pm$0.021]	[60]
CP Eri[31,32]	AMCVn	1740(84)	191.7021	-52.9098	0.218	10.5	[0.8$\pm$0.1]	[0.049$\pm$0.020]	[60]
SMSSJ0338[20]	DWD	1836.1(31.9)	128.8576	20.7792	-0.129	8.64	0.230 ± 0.015	$0.38^{+0.05}_{-0.03}$	69 ± 9
J2322+2103[19]	DWD	1918.08(21.60)	96.5151	-37.1844	0.071	8.81	0.291 ± 0.013	0.75 ± 0.26	[60]
SDSSJ0106[33]	DWD	2345.76(1.73)	191.9169	31.9952	-0.223	10.30	0.188 ± 0.011	$0.57^{+0.22}_{-0.07}$	67 ± 13
SDSSJ1630[34]	DWD	2388.0(6.0)	67.0760	43.3604	-0.147	9.54	0.298$\pm$0.019	0.76$\pm$0.24	[60]
J1526m2711[35]	DWD	2417.645(37.930)	340.4437	24.1935	-0.108	9.36	0.37 ± 0.02	$> 0.40 \pm 0.02$	[60]
SDSSJ1235[36,37]	DWD	2970.432(4.320)	284.5186	78.0320	-0.219	9.27	0.35 ± 0.01	$0.27^{+0.06}_{-0.02}$	27.0 ± 3.8
SDSSJ0923[38]	DWD	3883.68(43.20)	195.8199	44.7754	-0.236	8.62	0.275$\pm$0.015	0.76$\pm$0.23	[60]
CD–30°11223*[39]	sdB	4231.791855(155)	322.4875	28.9379	-0.388	4.55	0.54$\pm$0.02	0.79$\pm$0.01	82.9$\pm$0.4
SDSSJ1337[40]	DWD	5942.952(300)	89.0428	74.0799	0.306	11.31	0.51 ± 0.01	0.32 ± 0.01	13 ± 1
HD265435[41]	sdB	5945.917432(280)	87.0170	1.1225	-0.425	3.76	$0.63^{+0.13}_{-0.12}$	1.01 ± 0.15	64^{+14}_{-5}

[1]Strohmayer (2005), [2]Roelofs et al. (2010), [3]Burdge et al. 2019a, [4]Burdge et al. 2020b, [5]Ramsay et al. (2002), [6]Espaillat et al. (2005), [7]Brown et al. (2011), [8]Hermes et al. (2012), [9]Burdge et al. 2020a, [10]Green et al. (2018), [11]Skillman et al. (1999), [12]Roelofs et al. (2006), [13]Fontaine et al. (2011), [14]Kupfer et al. (2015), [15]Patterson et al. (2002) , [16]Roelofs et al. (2007a), [17]Brown et al. (2016b), [18]Kilic et al. (2014), [19]Brown et al. (2022), [20]Kilic et al. (2021), [21]Anderson et al. (2005), [22]Stella et al. (1987), [23]Chen et al. (2020), [24]Brown et al. (2020), [25]Burdge et al. (2019b), [26]Levitan et al. (2014), [27]Wevers et al. (2016), [28]Provencal et al. (1997), [29]Wood et al. (2002), [30]Levitan et al. (2011), [31]Howell et al. (1991), [32]Groot et al. (2001), [33]Kilic et al. (2011b), [34]Kilic et al. (2011a), [35]Kosakowski et al. (in prep), [36]Kilic et al. (2017), [37]Breedt et al. (2017), [38]Brown et al. (2010), [39]Geier et al. (2013), [40]Chandra et al. (2021), [41]Pelisoli et al. (2021), [42] M_V taken from van Paradijs & McClintock (1994)

In June 2022 Gaia data release 3 (DR3) was released. Gaia DR3 included the same data as eDR3 and as such astrometric solutions did not improve between eDR3 and DR3. However, DR3 included a large amount of additional information, including orbital astrometric solutions for wide binaries with a clean solution (Gaia Collaboration et al. 2022). For the remainder of the paper we will always refer to DR3 knowing that parallaxes and proper motions are the same for eDR3 and DR3.

3.2. *Distance estimation*

Gaia DR3 provides parallaxes which can be used to determine distances. To estimate distances from the measured parallaxes we use a probability-based inference approach (e.g. Bailer-Jones 2015; Igoshev et al. 2016; Astraatmadja & Bailer-Jones 2016; Bailer-Jones et al. 2018; Luri et al. 2018; Bailer-Jones et al. 2021). We follow a similar approach as described in detail in Sec. 3.2 in Kupfer et al. (2018). The measured parallax follows a probability distribution and with a prior on the true distance distribution for the observed sources we can constrain the distance even if the parallax has large uncertainties. If the parallax uncertainty is below 10% - 20% the distance estimate is independent of the prior. At larger uncertainties on the distance, the distance estimate becomes more and more dependent on the prior. We apply Bayes' theorem to measure the probability density for the distance:

$$P(r|\varpi, \sigma_\varpi) = \frac{1}{Z} \ P(\varpi|d, \sigma_\varpi) \ P(d), \tag{1}$$

where d is the distance, $P(\varpi|r, \sigma_\varpi)$ is the likelihood function, that can be assumed Gaussian (Lindegren et al. 2018). $P(r)$ is the prior and Z is a normalization constant. As in Kupfer et al. (2018) we adopt an exponentially decreasing volume density prior $P(d)$

$$P(d) = \begin{cases} \frac{d^2}{2L^3} \exp(-d/L) & \text{if } d > 0 \\ 0 & \text{otherwise}, \end{cases} \tag{2}$$

where $L > 0$ is the scale length. Compared to our previous study, here we assume two values for L based on the binary's membership to the thin or thick disc as detailed below. We also stress that for systems with poor parallax measurement, the distance estimate largely depends on our assumption for L.

To estimate if our candidate *LISA* binaries are members of the thin or thick disc, for each binary we calculate Galactic kinematics, i.e. velocity components and Galactic orbit. To do this, sky position, proper motions, systemic velocities, and distances are needed. We extract proper motions from Gaia DR3 and calculate the distance using Eqs. (1) and (2) by setting $L = 400\,\mathrm{pc}$ or $L = 795\,\mathrm{pc}$; these are typical values for L for thin disc and thick disc objects respectively[2]. Additionally, we use published systemic velocities, typically from radial velocity measurements. For systems with unknown systemic velocities, we assume $1\,\mathrm{km\,s^{-1}} \pm 50\,\mathrm{km\,s^{-1}}$. As for the distance estimate, we calculate Galactic kinematics assuming L values of $400\,\mathrm{pc}$ (thin discs) and $795\,\mathrm{pc}$ (thick disc). Using the Galactic potential of Allen & Santillan (1991) as revised by Irrgang et al. (2013), we calculate velocity in the direction of the Galactic center (V_ρ) and the Galactic rotation direction (V_ϕ), the Galactic orbital eccentricity (e), and the angular momentum in the Galactic z direction (J_z). The Galactic radial velocity V_ρ is negative towards the Galactic center, while stars that are revolving on retrograde orbits around the Galactic center have negative V_ϕ. Stars on retrograde orbits have positive J_z. Thin disk stars generally have very low eccentricities e. Population membership can be derived from the position in the V_ρ - V_ϕ diagram and the J_z - e diagram (Pauli et al. 2003, 2006). We find that for all objects the population membership is independent of the assumption for L and we apply the appropriate value for L for the distance estimation. Fig. 2 shows the population memberships for our candidate *LISA* sources. Most systems can be identified as thin disc objects. See Table 2 for the calculated distance with the assigned value for L.

3.3. *Gravitational wave parameter estimation*

Gravitational radiation for a typical stellar remnant binary at mHz frequencies can be modeled as a quasi-monochromatic signal characterized by 8 parameters: GW frequency f, heliocentric amplitude $\mathcal{A}$, frequency derivative $\dot{f}$, sky coordinates (λ, β), inclination angle ι, polarization angle ψ, and initial phase ϕ_0. The GW frequency and

---

[2] taken from the Gaia early data release 3 documentation https://gea.esac.esa.int/archive/documentation/GEDR3/Data_processing/chap_simulated/sec_cu2UM/ssec_cu2starsgal.html

Table 2. Measured EM properties (parallax, distance) and derived GW parameters of the verification binaries and detectable binaries. The distance for HM Cnc is assumed. The fractional error for the amplitude ($\sigma_\mathcal{A}/\mathcal{A}$) and the precision the inclination ($\Delta\iota$) is calculated for four years integration with *LISA*.

Source	f	ϖ DR3[a]	ϖ DR2[a]	L	d	$\sigma_\mathcal{A}/\mathcal{A}$	$\Delta\iota$
	(mHz)	(mas)	(mas)	(pc)	(pc)	(%)	(deg)
Verification binaries							
HM Cnc	6.220	-	-		[5000 − 10,000]	9.5	21
ZTFJ1539	4.822	-0.4926 ± 0.5726	-0.1125 ± 0.7884	795	2469 ± 1253	1.1	0.6
ZTFJ2243	3.788	-1.2372 ± 0.6578	-1.5658 ± 1.0522	400	1756 ± 726	0.36	0.6
V407 Vul	3.512	0.0978 ± 0.2384	0.0949 ± 0.3272	400	2089 ± 684	2.0	1.9
ES Cet	3.225	0.5606 ± 0.0677	0.5961 ± 0.1081	795	1779 ± 234	2.2	2.1
SDSSJ0651	2.614	1.0071 ± 0.3091	1.0002 ± 0.4759	400	958 ± 370	1.8	0.9
ZTFJ0538	2.308	0.9617 ± 0.2866	1.1477 ± 0.4811	400	999 ± 366	2.8	1.5
SDSSJ1351	2.130	0.6584 ± 0.2197	0.5957 ± 0.3134	795	1530 ± 755	27.9	33
AM CVn	1.944	3.3106 ± 0.0303	3.3512 ± 0.0452	795	302 ± 3	12.5	23
ZTFJ1905	1.938	1.8652 ± 1.5428	-	400	697 ± 605	11.6	35
SDSSJ1908	1.843	1.0232 ± 0.0335	0.9542 ± 0.0464	400	977 ± 32	19.5	30
HP Lib	1.814	3.5674 ± 0.0313	3.6225 ± 0.0525	400	280 ± 3	13.3	24
SDSSJ0935	1.683	2.7034 ± 0.6648	-	400	395 ± 203	3.3	3.1
J1239-2041	1.481	1.0068 ± 0.2309	1.4054 ± 0.3297	400	972 ± 272	13.3	9.5
SDSSJ0634	1.257	2.3111 ± 0.0835	2.3578 ± 0.091	400	433 ± 16	19.4	28
V803 Cen	1.253	3.4885 ± 0.0599	-	400	287 ± 5	16.1	27
Detectable binaries							
4U 1820−30	2.920	-0.7676 ± 0.2164	-0.8199 ± 0.2065	-	7972 ± 277[c]	32.3	34
SDSSJ2322	1.665	1.1558 ± 0.2244	1.2869 ± 0.2830	400	859 ± 206	29.6	36
PTFJ0533	1.621	0.7902 ± 0.2396	0.4741 ± 0.4786	400	1173 ± 390	33.3	30
ZTFJ2029	1.597	0.1240 ± 0.9893	-1.4269 ± 1.4345	400	1095 ± 644	18.4	10
PTF1J1919	1.484	0.6229 ± 0.2385	0.5499 ± 0.3274	400	1364 ± 471	65.2	46
CXOGBSJ1751	1.456	0.8591 ± 0.1733	0.4994 ± 0.2130	400	1128 ± 258	48.4	41
ZTFJ0722	1.406	0.6996 ± 0.2457	0.4132 ± 0.3508	795	1461 ± 785	46.3	23
CR Boo	1.359	2.8438 ± 0.0367	-	400	351 ± 5	19.8	29
KL Dra	1.332	1.0817 ± 0.0989	1.0354 ± 0.1488	795	930 ± 91	65.4	49
PTF1J0719	1.245	1.1851 ± 0.2292	1.1436 ± 0.3009	400	840 ± 201	68.0	48
CP Eri	1.149	1.3451 ± 0.2759	0.6836 ± 0.9407	400	747 ± 203	82.6	55
SMSSJ0338	1.089	1.8675 ± 0.0562	1.8994 ± 0.0793	400	536 ± 16	43.2	40
J2322+2103	1.043	0.8261 ± 0.2503	0.6943 ± 0.3168	400	1134 ± 386	38.1	38
SDSSJ0106	0.853	1.2011 ± 0.4739	1.3521 ± 0.5726	400	824 ± 441	76.7	51
SDSSJ1630	0.837	1.1748 ± 0.1952	0.9366 ± 0.2704	400	848 ± 167	40.1	39
J1526m2711	0.827	1.6053 ± 0.1751	1.5683 ± 0.2203	400	625 ± 75	39.8	38
SDSSJ1235	0.673	2.2504 ± 0.1389	2.3319 ± 0.1660	400	446 ± 28	39.8	38
SDSSJ0923	0.515	3.4795 ± 0.0648	3.3397 ± 0.1052	400	288 ± 5	41.3	38
CD–30°11223	0.473	2.8198 ± 0.0516	2.9629 ± 0.0797	400	355 ± 7	67.8	46
SDSSJ1337	0.337	8.8007 ± 0.0440	8.6993 ± 0.0524	400	114 ± 1	32.1	35
HD265435	0.336	2.1666 ± 0.0554	2.1994 ± 0.0628	400	461 ± 12	70.6	54

[a]Gaia Collaboration et al. (2018), [b]Gaia Collaboration et al. (2020), [c]Baumgardt & Vasiliev (2021)

amplitude are given by

$$f = 2/P_{\rm orb}, \tag{3}$$

with $P_{\rm orb}$ being the binary's orbital period, and

$$\mathcal{A} = \frac{2(G\mathcal{M})^{5/3}}{c^4 d}(\pi f)^{2/3}. \tag{4}$$

This is set by the binary's distance d and chirp mass

$$\mathcal{M} = \frac{(m_1 m_2)^{3/5}}{(m_1 + m_2)^{1/5}}, \tag{5}$$

for component masses m_1 and m_2. The frequency derivative $\dot{f}$ is expected to follow the gravitational radiation equation:

$$\dot{f} = \frac{96}{5}\frac{(G\mathcal{M})^{5/3}}{\pi c^5}(\pi f)^{11/3}. \tag{6}$$

To forecast *LISA* observations of the known binaries we use the VBMCMC sampler in LDASOFT (Littenberg et al. 2020). The sampler uses a parallel tempered Markov Chain Monte Carlo algorithm with delta-function priors on the orbital period and sky location of the binary based on the EM observations (cf. Table 1). The priors on the remaining parameters are uniform in log amplitude and cosine inclination. The sampler is also marginalizing over the first time derivative of the frequency, polarization angle, and initial phase of the binary, all of which are considered nuisance parameters for this study. Because this is a targeted analysis of known binaries the trans-dimensional sampling capabilities in LDASOFT are disabled and the algorithm uses a single template to recover the signal – effectively a delta function prior on the model. In this configuration, results for binaries below the detection threshold are used to set upper limits on the GW amplitude parameter.

The data being analyzed are simulated internally by VBMCMC and include stationary Gaussian noise with the same instrument noise spectrum as was used for the *LISA* Data Challenges (LDCs) in Challenge 2a[3] plus an estimated astrophysical foreground from the unresolved Galactic binaries as described in Cornish & Robson (2017). The analysis ignores any correlations, contamination, or additional statistical uncertainty caused by the presence of other signals in the data, and also treats the astrophysical foreground as a stationary noise source. Relaxing these simplifying assumptions will be most relevant for binaries where the astrophysical foreground dominates the instrument noise spectrum at GW frequencies $\lesssim$3 mHz but is currently beyond the scope of this analysis (considering overlap with other sources) or capabilities of the sampling algorithm (considering non-stationary noise).

4. RESULTS

We analyze 48 verification binary candidates in total using the VBMCMC sampler in LDASOFT for increasingly longer *LISA* mission science operation time: 1, 3, 6, 12, 36 and 48 months. We remind the reader that we perform a "targeted" analysis by fixing – using delta-function priors – binary's sky position and orbital period to the values provided by EM measurements; additionally, we marginalize over $\dot{f}$, ψ and ϕ_0 (cf. Section 3.3). Differently from our previous work to assess the detectability of a binary, instead of evaluating the signal-to-noise ratio we look at the binary's GW parameters posterior samples. We consider the binary as *detectable* if the GW amplitude parameter is constrained away from the minimum value allowed by the prior. This is most readily identifiable by looking at the two dimensional posterior distribution in the GW amplitude-inclination plane, where a detectable binary will have closed contours in the posterior. We call as *verification binary* a system that becomes detectable (as explained in Sec. 1) within 3 months of observation time with *LISA* and we call as *detectable binary* when it is detected after 48 months of observation time with *LISA*. We introduce this distinction to highlight the use of verification binaries for the early data validations, e.g. in preparation for the first data release. Our results show that an integration time as short as 1-3 months would allow for basic consistency tests on the recovered parameters on a few epochs of commissioning data for 6 - 16 verification binaries; while extending our definition up to 6 month increases the sample by only a few binaries. To clarify the difference between a verification, detectable and non-detectable binary, in Fig. 3 we show posteriors of the binary's inclination and GW amplitude for three examples: ZTFJ1539 ($\sim$ 7 min orbital period, verification binary),
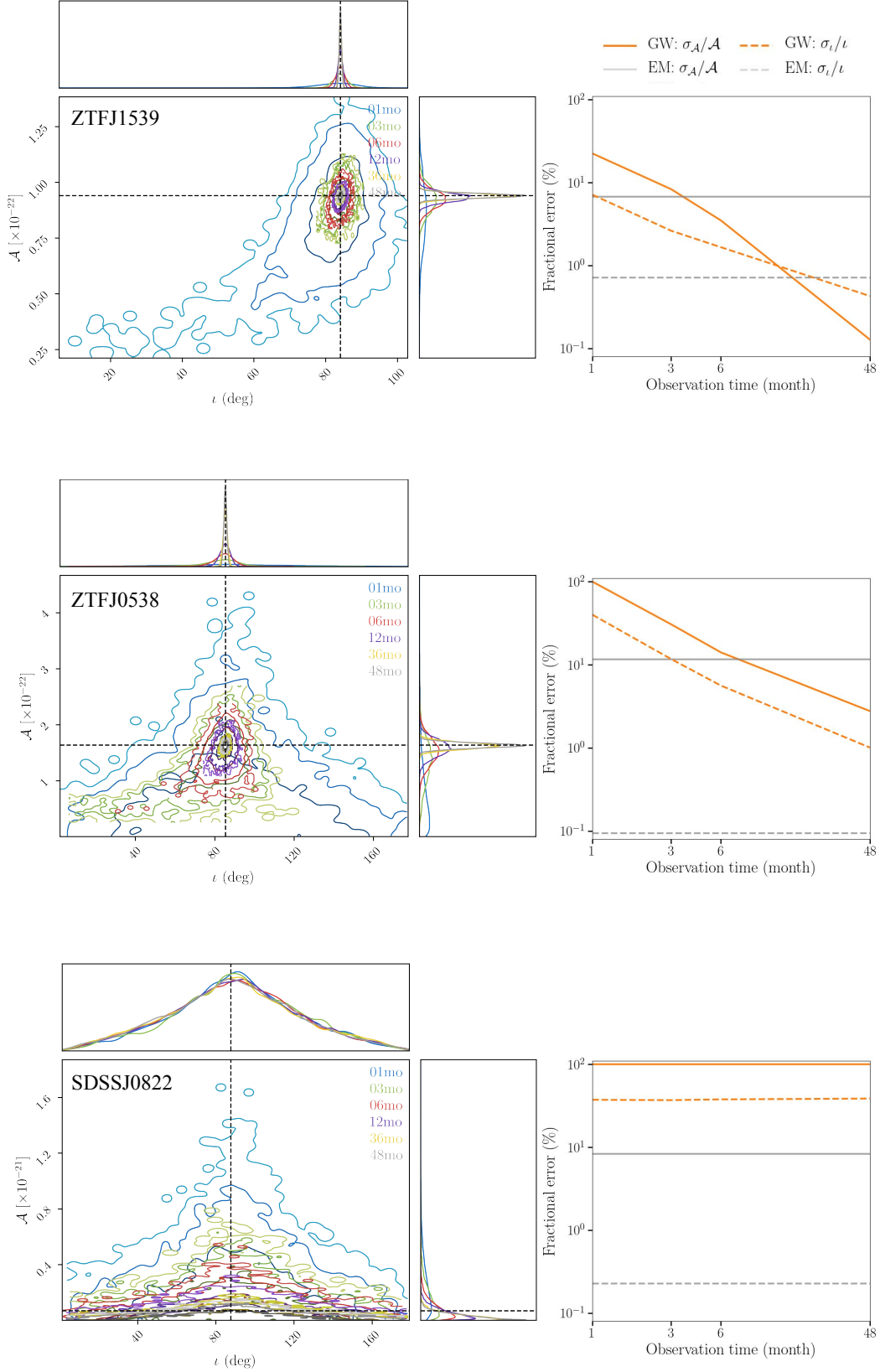
Figure 3. Three examples of posteriors for binary's inclination and GW amplitude; from top to bottom these are: ZTFJ1539 (verification binary), ZTFJ0538 (detectable binary) and SDSSJ0822 (non-detectable binary). On the left we show how the estimated fractional error on the amplitude $\sigma_{\mathcal{A}}/\mathcal{A}$ and inclination σ_{ι}/ι change as the functions of observation time; for comparison we also show current EM constrains and assuming that these won't change before *LISA*'s launch (cf. Table 1 and 2).
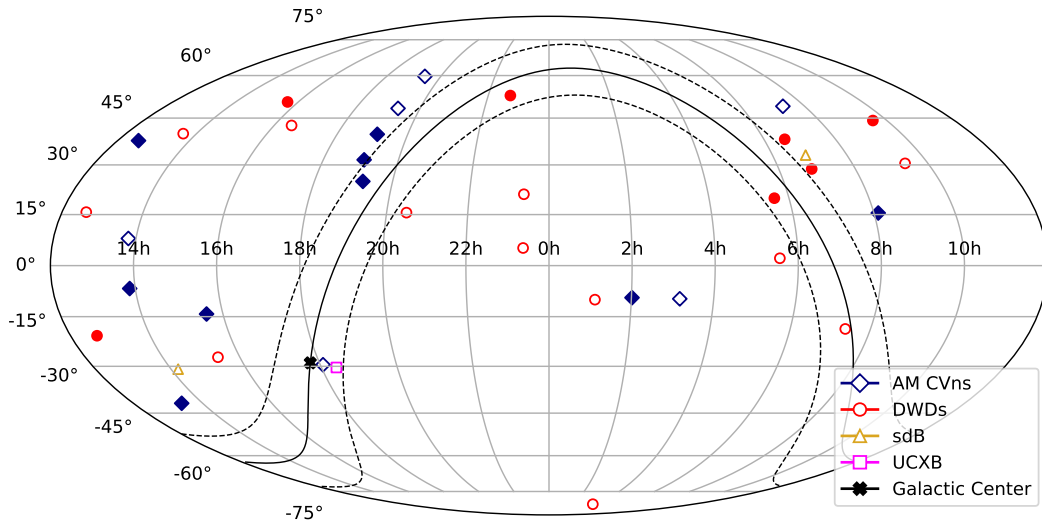
Figure 4. The position of the *LISA* binaries on the sky in an equatorial projection, with the Galactic plane ($\pm XX\circ$) shown by the full and dashed lines . Filled symbols are verification binaries whereas open symbols are detectable binaries.
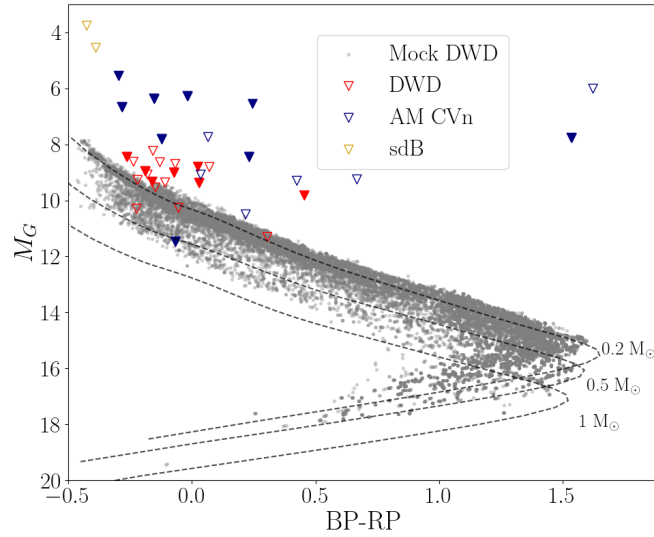
Figure 5. The position of verification binaries on the *Gaia* Hertzsprung-Russell diagram shows a clear bias in the current sample towards the brightest and bluest binaries. Down-pointing triangles are used to symbolize that absolute magnitude estimates are to be interpreted as upper limits because we do not account for extinction. Grey points in the background represent DWD Galactic mock population (Korol et al. 2017; Wilhelm et al. 2021). Dashed black lines show (single) Hydrogen-atmosphere white cooling tracks for a reference. Note that AM CVns cannot be directly compared to DWD and/or WD cooling models as for these binaries there is extra luminosity coming from accretion. As before, filled symbols represent verification binaries whereas open symbols represent detectable binaries
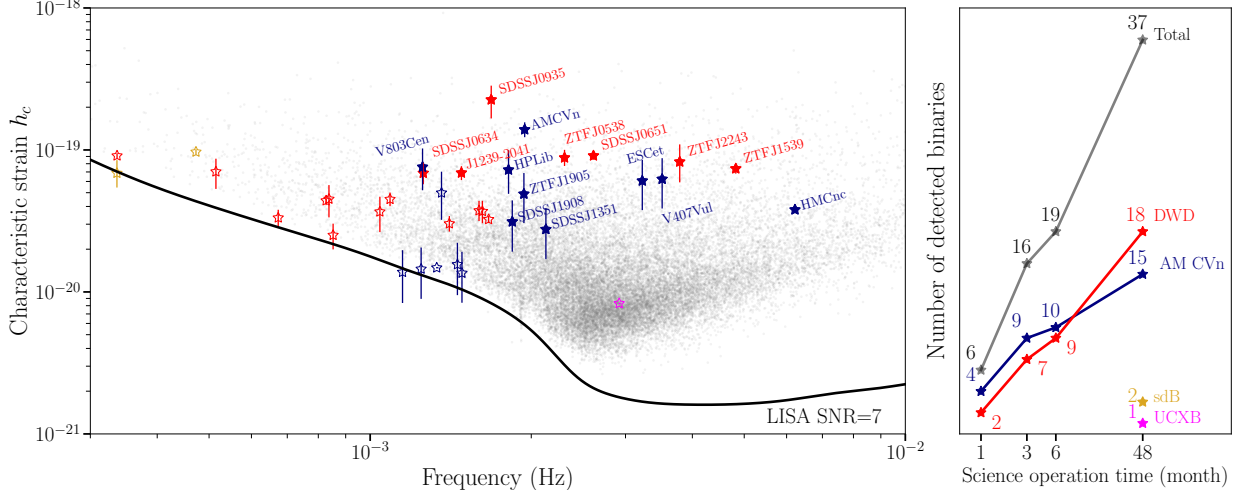
Figure 6. *Left panel:* Characteristic strain - frequency plot for detectable and verification binaries: AM CVns in blue, DWDs in red, sdBs in yellow and UCXB in magenta. Filled stars represent binaries detectable within 3 month of observations, which we call here 'verification binaries'. The error bars on characteristic strain show 1σ uncertainty evaluated by generating random samples from EM measurement uncertainties on binary component masses and distances presented in Table 1 and 2. Black solid line represents *LISA*'s sensitivity curve that accounts for the instrumental noise (LISA Science Study Team 2018) and Galactic confusion foreground (Babak et al. 2017). For comparison in gray we show a mock Galactic DWD population detectable with *LISA* from Wilhelm et al. (2021). *Right panel:* Number of detected binaries as a function of science operation time.

ZTFJ0538 ($\sim 15\,\mathrm{min}$, detectable binary) and SDSSJ0822 ($\sim 40\,\mathrm{min}$, non-detectable binary). ZTFJ1539 shows closed contours already after 1 month of observations, which become increasingly narrow as observation time increases. Being detectable so early on, it is highly likely that ZTFJ1539 can be used as one of *LISA's* verification binary. ZTFJ0538 represents an intermediate case as initially its posterior contours are open at low amplitude, but they close after 3 months at which point we classify this binary as detectable. Finally, we show the case of SDSSJ0822 which, based on the same reasoning as above, we classify as non detectable.

for the posterior distribution for all *LISA* sources). Right panels of Fig. 3 illustrate how *LISA*'s fractional error on GW amplitude $\mathcal{A}$ and inclination ι (orange lines) improve over time. Assuming that EM measurement would not improve in the future, which is plausible if no additional EM measurements will taken between now and when *LISA* will fly, we show the estimate of the same parameters based on the current EM measurement (gray lines) for comparison.

Based on our definition above, overall we find 37 binaries detectable with *LISA* within 4 yr of science operations, out of which we classify 16 (9 AM CVns + 7 DWDs) as verification binaries, i.e. detectable within the first 3 months. We list their properties in Table 1 and 2. The summary of our results is presented in Fig. 6. In the left panel we show characteristic strain - frequency plot for all detectable binaries: AM CVns in blue, DWDs in red, sdBs in yellow and UCXB in magenta. Filled stars represent *LISA* verification binaries, empty stars are detectable binaries within the nominal mission life time (48 month). We compute the error bars on characteristic strain by generating random samples from EM measurement uncertainties on binary component masses and distance (cf. Table 1 and 2); in the figure we plot 1σ uncertainty based on our random samples. For comparison we also show a mock Galactic DWD population of Wilhelm et al. (2021) in gray, as well as the *LISA* sensitivity curve at SNR=7 as black solid line. The comparison reveals that the current sample of known binaries is mainly representative of the 'loudest' GW sources in the Milky Way, while the majority is yet to be discovered in more remote parts of our Galaxy inaccessible for EM observatories. In the right panel of Fig. 6 we show the detection statistic as a function of the science operation time with a break down for different types of binaries showing that in increased science operation for *LISA* will lead to a larger number of detected binaries in the *LISA* data.

In our previous study (Kupfer et al. 2018), we identified only 13 detectable binaries. The reasons for the difference are multiple. Firstly, the sample of candidate verification binaries has tripled in the past few years (cf. Section 2). Secondly, some distance estimates have improved between *Gaia* DR2 and DR3 (this is, for example, true for CXOGBSJ1751 and SDSSJ163); for some binaries (SDSSJ0935, V803 Cen, CR Boo) parallaxes were not available as part of the

DR2. Most importantly, we also change our criterion for the detectability moving away from a SNR based definition. Recently, Finch et al. (2022) have used our catalog for a number of *LISA* data analysis investigations by performing a Bayesian parameter estimation with the BALROG code (Roebber et al. 2020; Buscicchio et al. 2021; Klein et al. 2022). They verified that binaries with SNR<6 generally display broad posteriors, with no clear peaks and with amplitude parameter being inconsistent with zero. Thus, they adopted the signal-to-noise threshold of 6 as criterion for the detectability with *LISA*. They found that up to 14 binaries can be detected within 3 months of observations (see their figures 4 and B1). This result is in agreement with our considering that the extra two binaries resulting detectable within 3 month (SDSSJ1351 and SDSSJ1908) in our study can be explained when taking into account the differences in the data analysis.

We report estimated fractional error on the GW amplitude ($\sigma_\mathcal{A}/\mathcal{A}$) and the estimated precision for the inclination ($\Delta\iota$) that can be reached after 4 years of observation in Table 2. On average, for verification binaries the amplitude is forecasted to be measured to $\sim 10\%$, while the inclination is expected to be determined with $\sim 15°$ precision. For detectable binaries these average errors decrease to $\sim 50\%$ and to $\sim 40°$ respectively. From the table one can deduce that the measurements depend on the binary's frequency (generally improving with increasing frequency) and strength of the signal (with verification binaries being better characterized than detectable binaries). Our estimates are in good agreement with Finch et al. (2022, see their table 2).

Figures 4 and 5 illustrate respectively the position of detectable (empty symbols) and verification (filled symbols) binaries on the sky and on the *Gaia* Hertzsprung-Russell diagram (HRD). Both reveal different limitations of this sample. Figure 4 shows that although the size of the candidate *LISA* binaries is progressively growing, it is biased towards the Northern Hemisphere (where the majority of surveys have been conducted so far), and to high latitudes (to avoid the dust extinction and crowding in the Galactic plane). From observations of bright non-degenerate stars we know that the Galactic stellar population is concentrated in the disc (region in between dashed lines) peaking towards the Galactic Center (thick black cross in Fig. 4), and so we expect *LISA* detectable binaries to follow the same distribution (e.g. see Nelemans et al. 2004). Figure 5 illustrates the bias towards the brightest and bluest binaries when comparing the absolute magnitudes (M_G) and colors (BP-RP) across our sample to the expected underlying population (gray points) of *LISA* detectable binaries. These have been evaluated using (single) WDs with hydrogen-atmosphere cooling models[4]; we show some of these cooling tracks for a reference. Note however that AM CVns cannot be directly compared to WD cooling models as for these binaries there is extra luminosity coming from accretion (Roelofs et al. 2007b; Carter et al. 2012, 2014). We note that on the HRD we use down-pointing triangles to highlight that our absolute magnitude estimates are to be interpreted as upper limits given that for all binaries in our sample because the extinction – necessary to convert apparent G magnitudes measured by *Gaia* magnitudes into absolute magnitudes M_G – is not well measured. *LISA* binaries on the white dwarf cooling tracks are intrinsically faint and with current surveys can only observed up to $\approx 1\,$kpc which limits the volume where *LISA* binaries can be detected. Additionally, in contrast to EM searches, *LISA* measures directly the amplitude of GW waves, rather than the energy flux. Thus, the observed GW signal scales as $1/d$, rather than $1/d^2$, allowing *LISA* to detect binaries at larger distances than in the traditional EM observational bands.

5. DISCUSSION

In this section we discuss the current sample of *LISA* verification and detectable binaries focusing on some systems more in detail. We also provide a future outlook highlighting on what measurements EM studies should focus more in order to maximize the scientific output for this sample.

5.1. *Improvements and updates to Gaia DR2*

Since Gaia DR2 several systems have now a published parallax. This includes ZTFJ1905, SDSSJ0935, V803 Cen and CR Boo. The only remaining system with no parallax measurement is HM Cnc. Therefore the distance estimate of HM Cnc is still highly uncertain. Roelofs et al. (2010) estimated a distance of 5 kpc based on its properties whereas Reinsch et al. (2007) estimated a distance of $\approx 2\,$kpc based on the observed flux. Most recently Munday et al. (2023) presented the discovery of $\ddot{f} = (-5.38 \pm 2.10) \times 10^{-27} \mathrm{Hz\,s^{-2}}$ in HM Cnc. They concluded that HM Cnc is close to the period minimum and theoretical MESA calculations find a mass of $\approx 1\,M_\odot$ for the accretor and $\approx 0.17\,M_\odot$ for the donor. This result is in strong contradiction to the results presented in Roelofs et al. (2010) based on a spectroscopic analysis.

---

[4] White dwarf cooling models are freely available at https://www.astro.umontreal.ca/~bergeron/CoolingModels/

Munday et al. (2023) also discussed different ways to measure the distance to HM Cnc and found values between 2 kpc and 11 kpc. This shows the very large uncertainties of the system properties from EM studies. Therefore, the expected GW amplitude remains uncertain. However, we predict that even at a distance of 10 kpc, HM Cnc will be detected within the first three months observations and so of *LISA* will provide an independent measurement of its distance.

We find that 20 *LISA* binaries from our list of have parallax precision better than 20%. For these binaries the inferred distances are independent of the assumed scale length prior. Note that our list also contains six binaries with either a negative parallax or a parallax error close to 100%. These are ZTF J1539, ZTF J2243, V407 Vul, ZTF J1905, 4U 1830-30, and ZTF J2029. For there cases the distance estimate is dominated by the derived scale length prior. Our distance estimates for ZTF J1539, ZTF J2243, and ZTF J2029 are consistent with the spectroscopic distance (Burdge et al. 2020a,b) giving further confidence in the assume prior.

4U 1830−30 is located in the globular cluster NGC 6624 which allows for an independent distance estimate using color-magnitude diagrams with theoretical isochrones, or by using variable stars that follow known relations between their periods and absolute luminosities like RR Lyrae stars. NGC 6624 has a well-measured distance of 7972 ± 277 pc (Baumgardt & Vasiliev 2021), which we take as the distance for 4U 1830−30.

V407 Vul's optical counterpart is dominated by a component that matches a G-type star with a blue variable (Steeghs et al. 2006). It is still unknown whether this is a chance alignment or whether V407 Vul is a triple system where an ultracompact inner binary is orbited by a G-star companion. Companions in orbits with a multi-year orbital period can present themselves in Gaia DR3 data, either they are listed in the non-single star tables of Gaia DR3 (**nss_two_body_orbit**) or they have a non-zero value in the **astrometric_excess_noise** keyword in the **gaia_source** table. The latter is non-zero if the astrometric solution shows additional perturbations to a single-source solution which could be an indication of a astrometric wobble if the G-star in V407 Vul is in a wide orbit (e.g. Belokurov et al. 2020; Penoyre et al. 2020). V407 Vul is not listed in the non-single star tables of Gaia DR3 (**nss_two_body_orbit**) and has an **astrometric_excess_noise**=0 and **astrometric_excess_noise_sig**=0 and therefore there is no indication in the current Gaia DR3 data set that the G-star is a wide companion to the inner ultracompact binary. However, we note that Gaia DR3 is only sensitive to few years periods. Longer periods would not yet show up as astrometric wobble and therefore we cannot exclude that the G-star has a period decades.

ZTF J1905 has an uncertain parallax in Gaia DR3 ($\varpi = 1.8652 \pm 1.5428$) and we find a distance of 697 ± 605 pc using $L = 400$ pc based on its Galactic kinematics. This results in an absolute magnitude of 11.47 mag which is inconsistent with AM CVn binaries with similar orbital periods such as AM CVn or SDSS J1908. In the orbital period range between 15 min - 20 min, AM CVn systems have typically absolute magnitudes around 6.5 mag. If ZTF J1905 has an absolute magnitude of 6.5 mag it would be located at around 6.5 kpc which is an order of magnitude inconsistent with our distance estimate from Gaia DR3 parallax. There is no indication in the Gaia DR3 quality keywords that the parallax is problematic. Additionally, there is only modest extinction towards the direction of ZTF J1905. Green et al. (2019) reports $E(g-r) = 0.18$ which results in an extinction of ≈ 0.5 mag in the Gaia$-G$ band which is not sufficient to explain the large discrepancy. However, if ZTF J1905 is located at 6.5 kpc it would not be a detectable *LISA* source.

5.2. *Limitations of the current sample*

The large number of different detection and analysis methods already led to a large non-uniformity in the way parameters of candidates *LISA* verification binaries are presented. Some binaries have system parameters presented with a 1−sigma error, while some have no constraints at all or only approximations (e.g. HM Cnc) or limits. Current efforts are ongoing to implement prior information from EM observations into GW analysis methods. However, the non-uniformity makes it non-trivial to implement the results from EM observations as priors in *LISA* data analysis for future multi-messenger studies. Therefore, it is crucial to develop uniform analysis methods for the different *LISA* binaries to provide a uniform set of prior information to allow for future uniform multi-messenger studies.

Despite the large progress of new systems over the last few years, the currently known sample is still very inhomogeneous and biased (see however Section 5.4). This is illustrated both in the sky distribution (Fig. 4) and the Hertzsprung Russell diagram (Fig. 5). The sky distribution is still biased towards the northern hemisphere with 60% of the known *LISA* sources having a positive declination. This fraction is still very similar to the sample of *LISA* binaries from Kupfer et al. (2018). However, we expect that this bias will improve over the next few years with the start of the ELM Survey South (Kosakowski et al. 2020) as well as the start of SDSS-V, BlackGEM and LSST which operate in the Southern hemisphere and Gaia DR4 which will provide photometry for all sky (see Sec. 5.4). The

Herzprung-Russel diagram also shows that most sources are above the main white dwarf track. Because ground based surveys discover magnitude limited samples, sources with a brighter absolute magnitude can be detected in a larger volume. A difference of two magnitudes leads an increase of detectable volume by a factor 15.8. That explains the large overabundance of sources above the white dwarf cooling track where most DWD *LISA* sources are expected. We predict that future surveys, such as LSST, Roman and possibly Euclid, with a larger limiting magnitude will be able to test a sufficiently large volume to be able to detect fainter sources on the white dwarf cooling track.

5.3. *Focus for future EM efforts*

When EM measurement of the binary's inclination is possible (mainly for nearly edge-on or edge-on systems, see Table 1), it generally provide an important prior input for *LISA*. In particular, Shah et al. (2012) have shown that an EM inclination measurement will help to improve the measurement of the GW amplitude, given a strong correlation between amplitude and inclination parameters in GW data (cf. Fig. 3). As a consequence, the chirp mass and the distance will be better constrained too. In addition, Finch et al. (2022) demonstrated that the effect of including EM prior information also contributes to a modest reduction in the time to detection compared to a blind search. Once the binary has been detected, further improvement depends on the inclination of the source. For face-on sources, prior knowledge of the inclination leads to a dramatic improvement in the amplitude measurement, which further improves as the observation time increases (see their figure 5). Thus, it is clear that prior knowledge of a binary's inclination from EM observations will be important for the future analysis of the *LISA* data. In the current sample 40% of the sources have no inclination measurement from EM observations. These are exclusively non-eclipsing sources where the measurement is non-trivial.

Constraining $\dot{f}$ from GW data alone may be challenging for low-frequency ($f < 2\,\mathrm{mHz}$) and/or low-signal-to-noise binaries accessible to *LISA* because this quantity is intrinsically small. Eclipsing sources are ideal to measure $\dot{f}$ with high-precision from ground based eclipse timing measurements. Long-baseline eclipse timing measurements (e.g. >10 years) may provide a very precise measurement of $\dot{f}$ to less than 1%. Shah & Nelemans (2014) demonstrated that adding EM information of $\dot{f}$ to the GW data analysis yield a more accurate constraint on the chirp mass. For example, $\dot{f}$ with 0.1% accuracy will constrain $\mathcal{M}$ to ∼0.11% accuracy for any inclination.

Prior knowledge of the distance (d) or parallax (ϖ) is also important for characterizing *LISA* binaries. As detailed in Section 3.2, parallax constrains the luminosity distance, which enters directly into GW amplitude (cf. Eq. 4). *LISA*'s measurement of GW frequency and amplitude combined with Gaia-based parallax allow the determination of the binary's chirp mass by solving Eq. (4) for $\mathcal{M}$. Note that this is without measuring $\dot{f}$, which is generally required to determine the chirp mass from GW data (cf. Eq. 6). Error propagation shows that the relation between the error on the chirp mass and that on the parallax is linear ($\sigma_{\mathcal{M}}/\mathcal{M} \propto \varpi\sigma_{\varpi}$). Thus, an improvement in the parallax measurement translates linearly into an improved estimate of the chirp mass measurement. Importantly, in this way one will be able to recover chirp masses for binaries at the low-frequency end of the LISA band, which may lack the measurement of $\dot{f}$, and for interacting binaries, whose $\dot{f}$ contains an astrophysical contribution (e.g. Breivik et al. 2018; Littenberg & Cornish 2019). This is especially interesting for the verification binaries AM CVn and HP Lib that already have a parallax and distance precision of ≈ 1% in the DR3. The upcoming DR4 - currently scheduled for the end of 2025 - will be based on 66 months of data collection, meaning that the improvement compared to the DR3 (based on 34 months of data) is expected to be significant. We can roughly estimate the improvement factor for the parallax errors compared to the errors released with DR3 as $\sigma_{\varpi} \propto (T_{\mathrm{DR3}}/T_{\mathrm{DR4}})^{0.5} \sim (34/66)^{0.5} \sim 0.7$, where T_{DR3} and T_{DR4} are expressed in month (Gaia Collaboration et al. 2018). Further improvements to the quality of the Gaia data are to be expected as the mission has been already given an indicative approval until the end of 2025[5], which implies that the data will be collected for up to 10 years in total.

5.4. *Future perspective for the sample of LISA binaries*

Between Gaia DR2 and Gaia DR3 the number of detectable *LISA* sources has more than doubled which can be explained by the large number of sky surveys that came online over the last few years. This will improve even more over the next decade with many additional surveys coming online over the next few years. As proven in the past photometric and spectroscopic surveys are ideal tools to find new *LISA* binaries and complement each other. Eclipses

---

[5] https://www.cosmos.esa.int/web/gaia/release

or tidal deformation lead to photometric variability on the orbital period, whereas compact *LISA* binaries show up in multi-epoch spectroscopy due to large radial velocity shifts between individual spectra.

SDSS-V is an all-sky, multi-epoch spectroscopic survey which started operations in 2020 and will provide spectra for a few million sources (Kollmeier et al. 2017). Already in early SDSS-V data Chandra et al. (2021) discovered a new detectable *LISA* binary. Other spectroscopic ongoing or upcoming spectroscopic surveys include LAMOST (Zhao et al. 2012), 4MOST (de Jong et al. 2019) or WEAVE (Dalton et al. 2014). The Asteroid Terrestrial-impact Last Alert System (ATLAS, Tonry et al. 2018; Heinze et al. 2018) and the Gravitational-wave Optical Transient Observer (GOTO, Steeghs et al. 2022) are ongoing photometric sky surveys with telescopes located in both hemispheres allowing for an all-sky coverage for both surveys. Their cadence and sky coverage are well suited to find *LISA* detectable binaries. BlackGEM is a photometric sky survey covering the Southern hemisphere expected to start observing in spring 2023 (Bloemen et al. 2015). Part of the BlackGEM operations will be the BlackGEM Fast Synoptic Survey which is a continuous high cadence survey of individual fields in the Southern hemisphere. The cadence is ideal to discover new *LISA* detectable binaries. First light for the Vera Rubin telescope is expected in 2024. The telescope will perform the Legacy Survey of Space and Time (LSST) covering the Southern hemisphere down to 24 mag (per single exposure) going much deeper and hence covering a significantly larger volume than current sky surveys. Although the cadence is expected to be not ideal for *LISA* binaries, LSST will collect sufficient photometric observations over 10 years to be able to discover *LISA* binaries. The next large Gaia data release (DR4) is expected to include precision time series photometry of ≈70 epochs for each object taken over five year time frame. Euclid is a space mission operating in the near-infrared and visible bands scheduled to be launched in 2023 with an unprecedented sky resolution of almost one order of magnitude better compared to ground based observatories. Part of Euclid's operation will be the Euclid deep survey covering a total of 40 sqd for three distinct fields. Each field will get several tens of epochs over its nominal mission time of six years with a depth of ≈ 25 mag for each epoch in the near-infrared bands (Laureijs et al. 2011). Finally, in the late 2020s the Nancy Roman space telescope will conduct a wide-field survey with the same sky resolution as Euclid down to 24 mag. Therefore, we expect that the number of LISA detectable sources will significantly increase before the *LISA* launches providing a large sample of multi-messenger sources (e.g. Korol et al. 2017; Li et al. 2020).

6. SUMMARY AND CONCLUSIONS

In this work we derive updated distances and Galactic kinematics for 48 verification binary candidates using parallaxes and proper motions from Gaia Data Release 3. Using these distances and system properties we calculate the detectability for each source after 1, 3, 6 and 48 months of *LISA* observations. We find that 16 verification binaries will be detected after 3 months of *LISA* observations and can be used for science verification. An additional 21 sources will be detected after 48 months of *LISA* observations totaling the number of detectable *LISA* to a total of 37 sources. The sources consist of 19 DWDs, 15 AM CVn binaries, two hot subdwarf binaries and one ultracompact X-ray binary. In particular AM CVn and HP Lib are verification binaries with parallax errors below 1% making them ideal validation sources. The number of detectable *LISA* binaries has tripled over the last four years since Kupfer et al. (2018). That is mainly due to increasing number of large scale sky surveys, in particular the ELM survey and ZTF were driving the discoveries over the last few years. However, even with the large increase in sources, the sample is still strongly biased towards luminous binaries and sources located in the Northern hemisphere. However, we predict that the number of systems will continue to increase significantly over the next few years with additional large scale surveys coming online over the next few years and strategies need to be developed to perform efficient follow-up for each source before *LISA* launches.

For sources without a measured $\dot{f}$, generally the distance is required to measure the chirp mass. The error on the parallax scales linearly with the error on the chirp mass. We find that the parallax precision has improved by $20\% - 30\%$ between Gaia DR2 and DR3 and another $\approx 30\%$ improvement is expected for Gaia DR4. We find that on average for verification binaries the gravitational wave amplitude is expected to be measured by *LISA* to $\approx 10\%$ precision, while the inclination is expected to be determined with $\approx 15°$ precision. For detectable binaries these average errors decrease to $\approx 50\%$ and to $\approx 40°$ respectively. Almost 40% of the *LISA* sources have no measured inclination from EM observations. These are non-eclipsing sources where it is non-trivial to measure an inclination angle and it might be that no progress will be made on the inclination before *LISA* gets launched. Therefore, even an uncertain inclination measurement from *LISA* will be valuable. Properties for all sources are collected for this publication is publicly available on the *LISA* Consortium GitLab repository https://gitlab.in2p3.fr/LISA/lisa-verification-binaries.

We wish to keep this list up-to-date for the Consortium and more broader community. Thus we welcome submission requests for new binaries and/or other suggestions.

7. ACKNOWLEDGMENTS

Facilities: Gaia

Software: astropy (Astropy Collaboration et al. 2013, 2018), LDASOFT (Littenberg et al. 2020)

REFERENCES

Allen, C., & Santillan, A. 1991, RMxAA, 22, 255

Amaro-Seoane, P., Audley, H., Babak, S., et al. 2017, arXiv e-prints, arXiv:1702.00786. https://arxiv.org/abs/1702.00786

Amaro-Seoane, P., Andrews, J., Arca Sedda, M., et al. 2022, arXiv e-prints, arXiv:2203.06016. https://arxiv.org/abs/2203.06016

Anderson, S. F., et al. 2005, AJ, 130, 2230, doi: 10.1086/491587

Astraatmadja, T. L., & Bailer-Jones, C. A. L. 2016, ApJ, 832, 137, doi: 10.3847/0004-637X/832/2/137

Astropy Collaboration, Robitaille, T. P., Tollerud, E. J., et al. 2013, A&A, 558, A33, doi: 10.1051/0004-6361/201322068

Astropy Collaboration, Price-Whelan, A. M., Sipőcz, B. M., et al. 2018, AJ, 156, 123, doi: 10.3847/1538-3881/aabc4f

Babak, S., Gair, J., Sesana, A., et al. 2017, Phys. Rev., D95, 103012, doi: 10.1103/PhysRevD.95.103012

Bailer-Jones, C. A. L. 2015, PASP, 127, 994, doi: 10.1086/683116

Bailer-Jones, C. A. L., Rybizki, J., Fouesneau, M., Demleitner, M., & Andrae, R. 2021, AJ, 161, 147, doi: 10.3847/1538-3881/abd806

Bailer-Jones, C. A. L., Rybizki, J., Fouesneau, M., Mantelet, G., & Andrae, R. 2018, AJ, 156, 58, doi: 10.3847/1538-3881/aacb21

Baumgardt, H., & Vasiliev, E. 2021, MNRAS, 505, 5957, doi: 10.1093/mnras/stab1474

Bellm, E. 2014, in The Third Hot-wiring the Transient Universe Workshop, ed. P. R. Wozniak, M. J. Graham, A. A. Mahabal, & R. Seaman, 27–33. https://arxiv.org/abs/1410.8185

Belokurov, V., Penoyre, Z., Oh, S., et al. 2020, MNRAS, 496, 1922, doi: 10.1093/mnras/staa152210.48550/arXiv.2003.05467

Bloemen, S., Groot, P., Nelemans, G., & Klein-Wolt, M. 2015, in Astronomical Society of the Pacific Conference Series, Vol. 496, Living Together: Planets, Host Stars and Binaries, ed. S. M. Rucinski, G. Torres, & M. Zejda, 254

Breedt, E., Steeghs, D., Marsh, T. R., et al. 2017, MNRAS, 468, 2910, doi: 10.1093/mnras/stx430

Breivik, K., Kremer, K., Bueno, M., et al. 2018, ApJL, 854, L1, doi: 10.3847/2041-8213/aaaa23

Breivik, K., Coughlin, S., Zevin, M., et al. 2020, ApJ, 898, 71, doi: 10.3847/1538-4357/ab9d85

Brown, W. R., Gianninas, A., Kilic, M., Kenyon, S. J., & Allende Prieto, C. 2016a, ApJ, 818, 155, doi: 10.3847/0004-637X/818/2/155

Brown, W. R., Kilic, M., Allende Prieto, C., & Kenyon, S. J. 2010, ApJ, 723, 1072, doi: 10.1088/0004-637X/723/2/1072

Brown, W. R., Kilic, M., Bédard, A., Kosakowski, A., & Bergeron, P. 2020, ApJL, 892, L35, doi: 10.3847/2041-8213/ab8228

Brown, W. R., Kilic, M., Hermes, J. J., et al. 2011, ApJL, 737, L23, doi: 10.1088/2041-8205/737/1/L23

Brown, W. R., Kilic, M., Kenyon, S. J., & Gianninas, A. 2016b, ApJ, 824, 46, doi: 10.3847/0004-637X/824/1/46

Brown, W. R., Kilic, M., Kosakowski, A., & Gianninas, A. 2022, ApJ, 933, 94, doi: 10.3847/1538-4357/ac72ac

Burdge, K. B., Coughlin, M. W., Fuller, J., et al. 2019a, Nature, 571, 528, doi: 10.1038/s41586-019-1403-0

Burdge, K. B., Fuller, J., Phinney, E. S., et al. 2019b, ApJL, 886, L12, doi: 10.3847/2041-8213/ab53e5

Burdge, K. B., Prince, T. A., Fuller, J., et al. 2020a, ApJ, 905, 32, doi: 10.3847/1538-4357/abc261

Burdge, K. B., Coughlin, M. W., Fuller, J., et al. 2020b, ApJL, 905, L7, doi: 10.3847/2041-8213/abca91

Buscicchio, R., Klein, A., Roebber, E., et al. 2021, PhRvD, 104, 044065, doi: 10.1103/PhysRevD.104.044065

Carter, P. J., Marsh, T. R., Steeghs, D., et al. 2012, MNRAS, 392, doi: 10.1093/mnras/sts485

Carter, P. J., Gänsicke, B. T., Steeghs, D., et al. 2014, MNRAS, 439, 2848, doi: 10.1093/mnras/stu142

Chandra, V., Hwang, H.-C., Zakamska, N. L., et al. 2021, ApJ, 921, 160, doi: 10.3847/1538-4357/ac2145

Chen, W.-C., Liu, D.-D., & Wang, B. 2020, ApJL, 900, L8, doi: 10.3847/2041-8213/abae66

Cornish, N., & Robson, T. 2017, Journal of Physics: Conference Series, 840, 012024, doi: 10.1088/1742-6596/840/1/012024

Dalton, G., Trager, S., Abrams, D. C., et al. 2014, in Society of Photo-Optical Instrumentation Engineers (SPIE) Conference Series, Vol. 9147, Ground-based and Airborne Instrumentation for Astronomy V, ed. S. K. Ramsay, I. S. McLean, & H. Takami, 91470L, doi: 10.1117/12.2055132

de Jong, R. S., Agertz, O., Berbel, A. A., et al. 2019, The Messenger, 175, 3, doi: 10.18727/0722-6691/5117

Espaillat, C., Patterson, J., Warner, B., & Woudt, P. 2005, PASP, 117, 189, doi: 10.1086/427959

Finch, E., Bartolucci, G., Chucherko, D., et al. 2022, arXiv e-prints, arXiv:2210.10812. https://arxiv.org/abs/2210.10812

Fontaine, G., et al. 2011, ApJ, 726, 92, doi: 10.1088/0004-637X/726/2/92

Gaia Collaboration, Brown, A. G. A., Vallenari, A., et al. 2020, arXiv e-prints, arXiv:2012.01533. https://arxiv.org/abs/2012.01533

Gaia Collaboration, Prusti, T., de Bruijne, J. H. J., et al. 2016, A&A, 595, A1, doi: 10.1051/0004-6361/201629272

Gaia Collaboration, Brown, A. G. A., Vallenari, A., et al. 2018, A&A, 616, A1, doi: 10.1051/0004-6361/201833051

Gaia Collaboration, Vallenari, A., Brown, A. G. A., et al. 2022, arXiv e-prints, arXiv:2208.00211. https://arxiv.org/abs/2208.00211

Geier, S., Marsh, T. R., Wang, B., et al. 2013, A&A, 554, A54, doi: 10.1051/0004-6361/201321395

Green, G. M., Schlafly, E., Zucker, C., Speagle, J. S., & Finkbeiner, D. 2019, ApJ, 887, 93, doi: 10.3847/1538-4357/ab5362

Green, G. M., Schlafly, E. F., Finkbeiner, D., et al. 2018, MNRAS, 478, 651, doi: 10.1093/mnras/sty1008

Groot, P. J., Nelemans, G., Steeghs, D., & Marsh, T. R. 2001, ApJL, 558, L123, doi: 10.1086/323605

Harms, J., Ambrosino, F., Angelini, L., et al. 2021, ApJ, 910, 1, doi: 10.3847/1538-4357/abe5a7

Heinze, A. N., Tonry, J. L., Denneau, L., et al. 2018, AJ, 156, 241, doi: 10.3847/1538-3881/aae47f

Hermes, J. J., Kilic, M., Brown, W. R., et al. 2012, ApJL, 757, L21, doi: 10.1088/2041-8205/757/2/L21

Howell, S. B., Szkody, P., Kreidl, T. J., & Dobrzycka, D. 1991, PASP, 103, 300, doi: 10.1086/132819

Huang, S.-J., Hu, Y.-M., Korol, V., et al. 2020, PhRvD, 102, 063021, doi: 10.1103/PhysRevD.102.063021

Hulse, R. A., & Taylor, J. H. 1975, ApJL, 195, L51, doi: 10.1086/181708

Igoshev, A., Verbunt, F., & Cator, E. 2016, A&A, 591, A123, doi: 10.1051/0004-6361/201527471

Irrgang, A., Wilcox, B., Tucker, E., & Schiefelbein, L. 2013, A&A, 549, A137, doi: 10.1051/0004-6361/201220540

Kilic, M., Brown, W. R., Bédard, A., & Kosakowski, A. 2021, ApJL, 918, L14, doi: 10.3847/2041-8213/ac1e2b

Kilic, M., Brown, W. R., Gianninas, A., et al. 2017, MNRAS, 471, 4218, doi: 10.1093/mnras/stx1886

—. 2014, MNRAS, 444, L1, doi: 10.1093/mnrasl/slu093

Kilic, M., Brown, W. R., Hermes, J. J., et al. 2011a, MNRAS, 418, L157, doi: 10.1111/j.1745-3933.2011.01165.x

Kilic, M., Brown, W. R., Kenyon, S. J., et al. 2011b, MNRAS, 413, L101, doi: 10.1111/j.1745-3933.2011.01044.x

Klein, A., Pratten, G., Buscicchio, R., et al. 2022, arXiv e-prints, arXiv:2204.03423. https://arxiv.org/abs/2204.03423

Kollmeier, J. A., Zasowski, G., Rix, H.-W., et al. 2017, arXiv e-prints, arXiv:1711.03234. https://arxiv.org/abs/1711.03234

Korol, V., Hallakoun, N., Toonen, S., & Karnesis, N. 2022, MNRAS, 511, 5936, doi: 10.1093/mnras/stac415

Korol, V., Rossi, E. M., Groot, P. J., et al. 2017, MNRAS, 470, 1894, doi: 10.1093/mnras/stx1285

Kosakowski, A., Kilic, M., & Brown, W. 2021, MNRAS, 500, 5098, doi: 10.1093/mnras/staa3571

Kosakowski, A., Kilic, M., Brown, W. R., & Gianninas, A. 2020, ApJ, 894, 53, doi: 10.3847/1538-4357/ab8300

Kupfer, T., Groot, P. J., Bloemen, S., et al. 2015, MNRAS, 453, 483, doi: 10.1093/mnras/stv1609

Kupfer, T., Korol, V., Shah, S., et al. 2018, MNRAS, 480, 302, doi: 10.1093/mnras/sty1545

18

Kupfer, T., Bauer, E. B., Marsh, T. R., et al. 2020a, ApJ, 891, 45, doi: 10.3847/1538-4357/ab72ff

Kupfer, T., Bauer, E. B., Burdge, K. B., et al. 2020b, ApJL, 898, L25, doi: 10.3847/2041-8213/aba3c2

Kupfer, T., Prince, T. A., van Roestel, J., et al. 2021, MNRAS, 505, 1254, doi: 10.1093/mnras/stab1344

Kupfer, T., Bauer, E. B., van Roestel, J., et al. 2022, ApJL, 925, L12, doi: 10.3847/2041-8213/ac48f1

Lamberts, A., Blunt, S., Littenberg, T. B., et al. 2019, MNRAS, 490, 5888, doi: 10.1093/mnras/stz2834

Laureijs, R., Amiaux, J., Arduini, S., et al. 2011, arXiv e-prints, arXiv:1110.3193, doi: 10.48550/arXiv.1110.3193

Levitan, D., Fulton, B. J., Groot, P. J., et al. 2011, ApJ, 739, 68, doi: 10.1088/0004-637X/739/2/68

Levitan, D., Kupfer, T., Groot, P. J., et al. 2014, ApJ, 785, 114, doi: 10.1088/0004-637X/785/2/114

Li, Z., Chen, X., Chen, H.-L., et al. 2020, ApJ, 893, 2, doi: 10.3847/1538-4357/ab7dc2

Lindegren, L., Hernandez, J., Bombrun, A., et al. 2018, ArXiv e-prints. https://arxiv.org/abs/1804.09366

LISA Science Study Team. 2018, LISA Science Requirements Document, Tech. Rep. ESA-L3-EST-SCI-RS-001, ESA. www.cosmos.esa.int/web/lisa/lisa-documents/

Littenberg, T. B. 2018, PhRvD, 98, 043008, doi: 10.1103/PhysRevD.98.043008

Littenberg, T. B., & Cornish, N. J. 2019, ApJL, 881, L43, doi: 10.3847/2041-8213/ab385f

—. 2023, arXiv e-prints, arXiv:2301.03673, doi: 10.48550/arXiv.2301.03673

Littenberg, T. B., Cornish, N. J., Lackeos, K., & Robson, T. 2020, Phys. Rev. D, 101, 123021, doi: 10.1103/PhysRevD.101.123021

Luo, J., Chen, L.-S., Duan, H.-Z., et al. 2016, Classical and Quantum Gravity, 33, 035010, doi: 10.1088/0264-9381/33/3/035010

Luri, X., Brown, A. G. A., Sarro, L. M., et al. 2018, ArXiv e-prints. https://arxiv.org/abs/1804.09376

Lyne, A. G., Burgay, M., Kramer, M., et al. 2004, Science, 303, 1153, doi: 10.1126/science.1094645

Marsh, T. R. 2011, Classical and Quantum Gravity, 28, 094019, doi: 10.1088/0264-9381/28/9/094019

Munday, J., Marsh, T. R., Hollands, M., et al. 2023, MNRAS, 518, 5123, doi: 10.1093/mnras/stac3385

Nelemans, G., & Jonker, P. G. 2010, NewAR, 54, 87, doi: 10.1016/j.newar.2010.09.021

Nelemans, G., Portegies Zwart, S. F., Verbunt, F., & Yungelson, L. R. 2001, A&A, 368, 939, doi: 10.1051/0004-6361:20010049

Nelemans, G., Yungelson, L. R., & Portegies Zwart, S. F. 2004, MNRAS, 349, 181, doi: 10.1111/j.1365-2966.2004.07479.x

Nissanke, S., Vallisneri, M., Nelemans, G., & Prince, T. A. 2012, ApJ, 758, 131, doi: 10.1088/0004-637X/758/2/131

Patterson, J., Fried, R. E., Rea, R., et al. 2002, PASP, 114, 65, doi: 10.1086/339450

Pauli, E. M., Napiwotzki, R., Altmann, M., et al. 2003, A&A, 400, 877, doi: 10.1051/0004-6361:20030012

Pauli, E.-M., Napiwotzki, R., Heber, U., Altmann, M., & Odenkirchen, M. 2006, A&A, 447, 173, doi: 10.1051/0004-6361:20052730

Pelisoli, I., Neunteufel, P., Geier, S., et al. 2021, Nature Astronomy, 5, 1052, doi: 10.1038/s41550-021-01413-0

Penoyre, Z., Belokurov, V., Wyn Evans, N., Everall, A., & Koposov, S. E. 2020, MNRAS, 495, 321, doi: 10.1093/mnras/staa114810.48550/arXiv.2003.05456

Petiteau, A. 2008, Theses, Université Paris-Diderot - Paris VII. https://theses.hal.science/tel-00383222

Provencal, J. L., Winget, D. E., Nather, R. E., et al. 1997, ApJ, 480, 383, doi: 10.1086/303971

Ramsay, G., Hakala, P., & Cropper, M. 2002, MNRAS, 332, L7, doi: 10.1046/j.1365-8711.2002.05471.x

Ramsay, G., Green, M. J., Marsh, T. R., et al. 2018, A&A, 620, A141, doi: 10.1051/0004-6361/201834261

Reinsch, K., Steiper, J., & Dreizler, S. 2007, in Astronomical Society of the Pacific Conference Series, Vol. 372, 15th European Workshop on White Dwarfs, ed. R. Napiwotzki & M. R. Burleigh, 419

Roebber, E., Buscicchio, R., Vecchio, A., et al. 2020, ApJL, 894, L15, doi: 10.3847/2041-8213/ab8ac9

Roelofs, G. H. A., Groot, P. J., Benedict, G. F., et al. 2007a, ApJ, 666, 1174, doi: 10.1086/520491

Roelofs, G. H. A., Groot, P. J., Marsh, T. R., Steeghs, D., & Nelemans, G. 2006, MNRAS, 365, 1109, doi: 10.1111/j.1365-2966.2005.09727.x

Roelofs, G. H. A., Nelemans, G., & Groot, P. J. 2007b, MNRAS, 382, 685, doi: 10.1111/j.1365-2966.2007.12451.x

Roelofs, G. H. A., Rau, A., Marsh, T. R., et al. 2010, ApJL, 711, L138, doi: 10.1088/2041-8205/711/2/L138

Ruan, W.-H., Guo, Z.-K., Cai, R.-G., & Zhang, Y.-Z. 2018, arXiv e-prints, arXiv:1807.09495. https://arxiv.org/abs/1807.09495

Ruiter, A. J., Belczynski, K., Benacquista, M., & Holley-Bockelmann, K. 2009, ApJ, 693, 383, doi: 10.1088/0004-637X/693/1/383

Savalle, E., Gair, J., Speri, L., & Babak, S. 2022, PhRvD, 106, 022003, doi: 10.1103/PhysRevD.106.022003

Shah, S., & Nelemans, G. 2014, ApJ, 790, 161, doi: 10.1088/0004-637X/790/2/161

Shah, S., van der Sluys, M., & Nelemans, G. 2012, A&A, 544, A153, doi: 10.1051/0004-6361/201219309

Skillman, D. R., Patterson, J., Kemp, J., et al. 1999, PASP, 111, 1281, doi: 10.1086/316437

Solheim, J. E. 2010, Publications of the Astronomical Society of the Pacific, 122, 1133, doi: 10.1086/656680

Steeghs, D., Marsh, T. R., Barros, S. C. C., et al. 2006, ApJ, 649, 382, doi: 10.1086/506343

Steeghs, D., Galloway, D. K., Ackley, K., et al. 2022, MNRAS, 511, 2405, doi: 10.1093/mnras/stac013

Stella, L., Priedhorsky, W., & White, N. E. 1987, ApJL, 312, L17, doi: 10.1086/184811

Ströer, A., & Vecchio, A. 2006, Classical and Quantum Gravity, 23, 809, doi: 10.1088/0264-9381/23/19/S19

Strohmayer, T. E. 2005, ApJ, 627, 920, doi: 10.1086/430439

Tauris, T. M. 2018, PhRvL, 121, 131105, doi: 10.1103/PhysRevLett.121.131105

Tonry, J. L., Denneau, L., Heinze, A. N., et al. 2018, PASP, 130, 064505, doi: 10.1088/1538-3873/aabadf

van Paradijs, J., & McClintock, J. E. 1994, A&A, 290, 133

van Roestel, J., Kupfer, T., Green, M. J., et al. 2022, MNRAS, 512, 5440, doi: 10.1093/mnras/stab2421

Weisberg, J. M., & Taylor, J. H. 2005, in Astronomical Society of the Pacific Conference Series, Vol. 328, Binary Radio Pulsars, ed. F. A. Rasio & I. H. Stairs, 25. https://arxiv.org/abs/astro-ph/0407149

Wevers, T., Torres, M. A. P., Jonker, P. G., et al. 2016, MNRAS, 462, L106, doi: 10.1093/mnrasl/slw141

Wilhelm, M. J. C., Korol, V., Rossi, E. M., & D'Onghia, E. 2021, MNRAS, 500, 4958, doi: 10.1093/mnras/staa3457

Wood, M. A., Casey, M. J., Garnavich, P. M., & Haag, B. 2002, MNRAS, 334, 87, doi: 10.1046/j.1365-8711.2002.05484.x

Zhao, G., Zhao, Y., Chu, Y., Jing, Y., & Deng, L. 2012, arXiv e-prints, arXiv:1206.3569, doi: 10.48550/arXiv.1206.3569